Hindawi
International Journal of Intelligent Systems
Volume 2023, Article ID 2768126, 22 pages
https://doi.org/10.1155/2023/2768126

Research Article

Decision Fusion and Micro-Doppler Effects in Moving Sonar Target Recognition

Farhan A. Alenizi,[1] **Omar Mutab Alsalami**,[2] **Abbas Saffari**,[3] **Seyed Hamid Zahiri**,[3] **and Mokhtar Mohammadi**[4]

[1]*Electrical Engineering Department, College of Engineering, Prince Sattam Bin Abdulaziz University, Al-Kharj 11942, Saudi Arabia*
[2]*Department of Electrical Engineering, College of Engineering, Taif University, P.O. Box 11099, Taif 21944, Saudi Arabia*
[3]*Department of Electrical Engineering, University of Birjand, Birjand, Iran*
[4]*Department of Information Technology, College of Engineering and Computer Science, Lebanese French University, Erbil, Kurdistan Region, Iraq*

Correspondence should be addressed to Abbas Saffari; abbas.saffari@birjand.ac.ir

Received 30 January 2023; Revised 20 September 2023; Accepted 19 October 2023; Published 2 November 2023

Academic Editor: Alexander Hošovský

This paper proposes a method for underwater target recognition based on micro-Doppler effects (called STR_MD) using a majority voting ensemble classifier weighted with particle swarm optimization (PSO) (called MV-PSO). The micro-Doppler effect refers to amplitude/phase modulation of the received signal by rotating parts of a target such as propellers. Since different targets' geometric and physical properties differ, their micro-Doppler signature is different. This inconsistency can be considered an effective issue (especially in the frequency domain) for sonar target recognition. To demonstrate the effectiveness of the proposed method, both simulated and practical micro-Doppler data are produced and applied to the designed STR_MD. Also, MV-PSO with six well-known basic classifiers, k-nearest neighbors (k-NN), Naive Bayes (NB), decision tree (DT), MLP_NN, support vector machine (SVM), and random forest (RF), has been used to evaluate the performance of the proposed method. This ensemble classifier assigns an instance to a class that most base classifiers agree on. However, basic classifiers in a set seldom work just as well. Therefore, in this case, one strategy is to weigh each classification depending on its performance using PSO. The performance parameters measured are the recognition score, reliability, and processing time. The simulation results showed that the correct recognition rate, reliability, and processing time for the simulated data at SNR = 5 dB and 10° viewing angle were 98.50, 98.89, and 9.81 s, respectively, and for the practical dataset with RPM = 1200, 100, 100, and 4.43, respectively. Thus, MV-PSO has a more encouraging performance in STR_MD for simulated and practical micro-Doppler sonar datasets.

1. Introduction

Due to the complex physical properties of sonar targets [1, 2], the subject of automatic classification and recognition of sonar targets has become one of the favorite fields of researchers and artisans' active in this field [3–5]. Recent studies show that artificial intelligence techniques are a practical solution to real-world [6–8] ocean engineering problems [9, 10]. Artificial intelligence models have significant features such as a high level of accuracy, flexibility, and inherent parallel structure [11]; therefore, they can lead to applications in ocean engineering problems [12, 13], especially in the classification of sonar targets [14]. Recently, classification has been investigated with two approaches. The first method is deterministic methods based on oceanography [15], sonar modeling and engineering [16], and statistical processing [17, 18]. The second method is stochastic methods with different applications that include predicting the oceanic phenomenon [19, 20], increasing feature extraction approaches [16, 21], and introducing new classification techniques [22]. It has been proven that the most famous

random method is using artificial intelligence techniques [23–25]. Using the first method requires costly investment in equipment, human resources, and logistics, while using the second method, in addition to reducing costs, reduces complexity [26, 27]. Machine learning is the most critical subset of artificial intelligence [28–30]. Supervised learning is the most appropriate method for classification problems [31, 32]. The learning algorithm calculates the training data output in this method iteratively. When the algorithm achieves an acceptable performance, an observer corrects these outputs, and the learning process stops [33–35].

Analysis of emitted audio signals from targets plays an influential role in classifying sonar targets using various artificial intelligence techniques [36–38]. The most propagated sound is emitted from the propeller area and its rotating parts [39–41]. It can be concluded from the in-depth research that has been performed so far on the techniques for automatically recognizing sonar targets that the only technique that has a suitable theory and mathematical model to simulate the reference target database is the technique that uses the rotation of sonar targets' rotating parts as a modulation signal. This method is known in the literature for automatic sonar target recognition as modulating rotating parts (called the micro-Doppler phenomenon) [42, 43]. The use of radar micro-Doppler for air and ground purposes is widespread; however, these phenomena are seldom used for sonar targets in the ocean and sea [44–46].

On the other hand, automatic target recognition (ATR) is also one of the most important applications of pattern recognition in computer science [47]. ATR systems operate in such a way that by employing different classifiers, they can recognize anonymous targets in the feature space [48, 49]. Given the breadth of the ATR topic, papers usually focus on one part of the ATR system. This paper used a new STR_MD method for simulating sonar datasets and increasing the performance (correct recognition rate and reliability) of an ATR system. On the other hand, sometimes, the presence of noise in the data causes the classifiers to make mistakes [50]. In this case, the fusion of decisions of different classifiers can reduce the error rate and increase system performance. In other words, using the votes of the majority of different classifiers can improve system performance. However, not all classifiers in the set have the same performance, and it is rare for them to have the same performance [51]. In this case, weighing the votes is the right strategy [50]. Weighing has a variety of techniques. One of the newest and most efficient weighting techniques is using heuristic algorithms.

An effective approach, which has not yet been applied in the field of micro-Doppler sonar signature analysis, is related to the use of an ensemble classifier that uses the MV-PSO technique. This specific technique represents notable novelty within the present research, thereby distinguishing it from prior studies.

The primary motivation driving this scientific inquiry lies in the exploration and investigation of the utilization of MV-PSO for STR_MD. This research aims to thoroughly examine the potential of MV-PSO as an effective and efficient methodology for STR_MD, thereby addressing a crucial gap in the existing scientific literature. By scrutinizing the applicability, performance, and underlying mechanisms of MV-PSO in the context of STR_MD, this study seeks to contribute valuable insights and advancements to the field of underwater target detection.

Therefore, it can be said that our main contribution to this article is as follows:

(i) Use of appropriate mathematical model and data acquisition based on micro-Doppler signature using the propeller specifications of real targets

(ii) Obtaining practical data at different RPMs by cavitation tunnel

(iii) Automatic recognition of sonar data by using the micro-Doppler signature and k-NN classifiers, DT, NB, MLP-NN, SVM, and RF

(iv) Using the ensemble classifier by MV-PSO (decision fusion)

(v) Generating optimal weight for votes of basic classifiers using PSO

(vi) Analysis of results by examining comparative parameters

The paper is organized as follows. Section 2 deals with the related works and background. Section 3 discusses using sonar micro-Doppler to recognize sonar targets automatically. Section 4 presents the simulated and practical dataset's experimental results. Section 5 concludes the study.

2. Related Works and Background

Many researchers have recently been interested in automated sonar target recognition due to its widespread commercial and military applications. Some current research studies are reported in Table 1.

The most challenging point in these references is their dataset. The only dataset we have access to is the simulated sonar dataset based on the micro-Doppler effect available in reference [44]. Other sonar datasets used in Table 1 can be divided into two subsets. The first subset is a collection of data collected during a practical test scenario at sea or in the ocean. Disadvantages of sonar datasets obtained from practical testing include unavailability, high cost, and lack of knowledge about the amount of SNR available at the test. The second subset is the sonar dataset obtained from the Gorman and Sejnowski experiment [63]. In this experiment, there are two types of echo, the first is related to a metal cylinder (plays the role of the real target), and the second is related to a rock of the same size as the cylinder (plays the role of the clutter or false target). Therefore, this sonar dataset is suitable for applications of detecting real targets from false targets. This experiment was performed at 4–15 dB SNRs, while the actual sea and ocean environment has a lot of unwanted signals. However, due to the unavailability of sonar datasets used in other articles and for the purpose of comparative comparison, in this article, the micro-Doppler dataset, the cavitation tunnel dataset, and the Gorman and Sejnowski dataset are used as the benchmark sonar dataset.

Table 1: Related work.

#	Reference	Default task	Classification model	Dataset
1	[52]	Feature selection	RBF-NN	Collected with the practical test scenario
2	[53]	Feature selection and classification	Few-shot learning (FSL)	Collected with the practical test scenario
3	[44]	Feature selection	k-NN	Simulated micro-Doppler and cavitation tunnel
4	[47]	Algorithmic development	Hybrid (RBF-NN + WOA + fuzzy system)	Collected with the practical test scenario
5	[54]	Algorithmic development	Hybrid (MLP-NN + GOA + fuzzy system)	Collected with the practical test scenario
6	[55]	Algorithmic development	Hybrid (MLP-NN + ChOA + fuzzy system)	Collected with the practical test scenario
7	[56]	Algorithmic development	Hybrid (RBF-NN + SCA)	Gorman and Sejnowski + common dataset 2015 (CDS2015) + real data collected by the sonobuoy
8	[57]	Algorithmic development	Hybrid (MLP-NN + GSA)	Real data collected by the sonobuoy
9	[58]	Algorithmic development	MLP + DA	Collected with the practical test scenario
10	[59]	Algorithmic development	Hybrid (MLP-NN + BBO)	Real data collected by sonobuoy and lense
11	[60]	Algorithmic development	Hybrid (MLP-NN + GWO)	Lense, Iris, Gorman, and Sejnowski
12	[61]	Classification	k-NN, SVM, and DT	Gorman and Sejnowski
13	[62]	Classification	Random forest, SVM, and k-NN	Collected with the practical test scenario

Reference [52] employs a feature extraction technique that combines cepstrum and STFT, coupled with a network RBF-NN. In reference [53], a method for concept extraction is introduced, utilizing STFT as the basis, along with the application of an FSL classifier for data classification. Moving to reference [44], a feature selection approach utilizing PSO is proposed, followed by classification using a k-NN classifier. Rows 4 to 11 of Table 1 demonstrate the utilization of an artificial neural network trained with a metaheuristic algorithm for classification purposes. Rows 12 and 13, on the other hand, employ well-known machine learning algorithms (k-NN, NB, DT, MLP_NN, SVM, and RF) for classification. However, each of these algorithms exhibits certain weaknesses. For instance, k-NN suffers from high computational cost and sensitivity to feature scaling, while NB heavily relies on the assumption of feature independence and struggles with rare events. DT is prone to overfitting, sensitive to data changes, and limited in modeling complex relationships. MLP-NN requires determining the optimal architecture, is sensitive to weight initialization, and can be time-consuming to train. SVM is sensitive to kernel selection, memory-intensive, and less efficient for large datasets. RF has a high computational complexity and requires careful parameter settings, such as the number of trees, tree depth, and the number of features considered at each split. Suboptimal parameter configurations can result in a less effective model.

The identified weaknesses in the mentioned algorithms serve as a strong motivation to develop a sonar target recognition system that employs a weighted majority voting approach enhanced by PSO. By addressing the limitations of individual classifiers, this system aims to improve classification recognition rate and reliability. The incorporation of PSO enables the determination of optimal weights assigned to each classifier, effectively leveraging their strengths and mitigating their weaknesses. Ultimately, the proposed system strives to enhance the overall performance and reliability of the sonar target recognition process.

2.1. Micro-Doppler Effect. Sidebands appear on the object's Doppler frequency due to micromotions such as vibrations or rotations of an object or a component on an object that affect the additional frequencies in the signal [44, 64]. Micro-Doppler sonar is the term used for this phenomenon. Recent studies have demonstrated that a target's micro-Doppler qualities may be used to recognize or classify it using micro-Doppler methods. In order to investigate an object's micro-Doppler characteristics, time-frequency analysis is performed to offer details on these local conditions over time and frequency [39]. Micromotion often has a recognizable signature on an object. Micromotion directly results from an object's dynamic motion characteristics, and micro-Doppler characteristics directly reflect micromotion. Nevertheless, utilizing an object's micro-Doppler signatures can classify objects with distinct dynamic motion characteristics [65].

2.1.1. Theory. The analytic signal of a pure tone $s(t)$ is defined as the signal $\hat{s}(t)$, such that $s(t) = ¼\ \text{real}(\hat{s}(t))$, and is generally expressed in the polar format as [66] follows:

$$\hat{s}(t) = e^{j2\pi f_0 t}. \tag{1}$$

The target's Doppler shift in relation to the sonar (or radar) system for a target moving at a constant radial velocity v is as follows:

$$f_D = 2f_0\frac{v}{C_s}, \tag{2}$$

where C_s is the speed at which sound moves through the water and f_0 is the carrier frequency of the active sensor. The Doppler shift is the total of each individual Doppler shift when the target consists of multiple M components, and each part moves at a velocity component $v_i(t)$.

$$f_D(t) = \sum_{i=1}^{M} 2f_0 \frac{v_i(t)}{C_s}. \tag{3}$$

The echo return's analytical signal for such a target is as follows:

$$\hat{s}_R(t) = e^{j2\pi f_0 t} \times e^{j2\pi f_D(t)t}. \tag{4}$$

The conjugates of the transmitted signal $\hat{s}(t)$ and the received signal $\hat{s}_R(t)$ are combined as follows:

$$\hat{s}_R(t) \times \hat{s}(t)^* = e^{j2\pi f_D(t)t}. \tag{5}$$

The abovementioned relation provides the possibility of the Doppler signature of the data. This is the main source of micro-Doppler information on the target that can be used to identify and classify the target. The available bandwidth is usually much less than the carrier frequency, with the information at lower frequencies. Equation (7) shows that the Doppler change is inversely proportional to the transmitted wavelength $\lambda = C_s/f_0$. However, compared to the speed of light, sound waves are at a far slower rate. Therefore, obtaining high Doppler shifts using acoustics is much easier than radio frequency devices. Short-term Fourier transforms can be used to represent micro-Doppler signatures in two-dimensional time-frequency space (STFT). This can be calculated by calculating the Fourier transform of a set of 50% sliding windows $x_i(n)$ with the overlap of a given length N. The velocity resolution is determined by the sampling rate of the DAQ and the window size of the STFT as in equation (6).

$$\mathrm{STFT}(i, K) = \sum_{n=0}^{N-1} x_i(n) e^{-j2\pi(nK/N)}. K = 0.1.2. \cdots . N-1, \tag{6}$$

where $x_i(n)$ is the i-th window and is equal to

$$x_i(n) = \hat{S}_R(k) \cdot w(n), \tag{7}$$

where $w(n)$ is a suitable weight function and k is obtained from the following equation:

$$\mathrm{k} = \mathrm{n} + \mathrm{i}\,\frac{N}{2}. \tag{8}$$

The frequency resolution can be approximated by the duration of a $T_w = N/f_s$ window, where f_s is the sampling rate. Therefore, only Doppler displacements greater than $1/T_w$ that match the velocities will be visible.

$$v > \frac{C_s}{2f_0 T_w}. \tag{9}$$

Equation (9) shows that the use of higher frequencies has the added advantage of inducing broader micro-Doppler bandwidth, and given the specific frequency resolution, it is easier to detect small movements when the carrier frequency is higher.

3. Usage of the Micro-Doppler Phenomenon in the Classification of Sonar Targets

Designing an automated sonar target recognition system entails a systematic approach akin to other pattern recognition systems. This process involves a series of four distinct steps, each contributing to the overall functionality and effectiveness of the system.

In Subsection 3.1, the procedure for sampling the sonar signal to extract the micro-Doppler effect is explicated. This step is crucial as it enables the system to capture and analyze the intricate micro-Doppler characteristics inherent in the sonar signal.

Moving forward, Subsection 3.2 focuses on establishing the reference targets utilized within the recognition system. Notably, this subsection identifies and delineates the various target types, including surface vessels, submarines, and torpedoes.

Subsection 3.3 introduces feature vectors that are derived from the sonar micro-Doppler phenomenon. These feature vectors serve as informative representations, encapsulating the distinctive characteristics and patterns exhibited by the targets. By leveraging the micro-Doppler effect, the system can discern subtle variations and discernible patterns, enhancing its discriminative capability.

Lastly, Subsection 3.4 sheds light on the classifiers employed in the automatic sonar target recognition system. These classifiers are fundamental components that facilitate the categorization and identification of the targets based on the extracted features. The introduction of the classifiers in this subsection underlines their pivotal role in the recognition process, enabling accurate and efficient target classification.

In summary, the design of an automatic sonar target recognition system involves a comprehensive approach comprising of four key steps. These steps encompass signal sampling, reference target establishment, feature vector extraction based on the micro-Doppler effect, and the utilization of classifiers. By following this systematic procedure, the system can effectively identify and classify diverse targets encountered in sonar applications.

3.1. Sample Rate. In some ways, the sampling rate is one of the essential parts of signal processing. If a reasonable sampling rate is not used, the sampling quality may be reduced and valuable information may be removed from the signal. Therefore, to maintain the quality and resolution of the signal in the range of [0–0.4] seconds, a sampling rate of 1 MHz was used.

3.2. Reference Targets. The absence of reliable data is one of the most severe issues in sonar research. In addition, unwanted signals and the sea's complex and dynamic environment provide a solid motivation for creating a simulated dataset using the mathematical model of the return signal from the moving sonar target propeller. The tested targets are listed in [44].

Different types of vessels have been used to select samples, including container vessels, tankers, passengers, cruises, autonomous underwater vehicles, tugboats, and different classes of navy ships, submarines, and military torpedoes, to evaluate the performance of the STR_MD.

3.3. Feature Vectors Based on Sonar Micro-Doppler Phenomenon. An appropriate mathematical model (10) was used to simulate the return signal from the rotating part (propeller) of sonar targets in order to create a data collection of return signals from the propeller of sonar targets, as explained in Subsection 3.2.

$$s_r(t) = \sum_{n=0}^{N-1} A_r (L_2 - L_1) e^{j(\beta)} \cdot \operatorname{sinc}\left(\frac{4\pi}{\lambda} \frac{(L_2 - L_1)}{2} \cos(\theta) \sin\left(\omega_r t + \frac{2\pi n}{N}\right)\right),$$
$$\beta = \omega_c t - \frac{4\pi}{\lambda}\left(R + vt + \frac{L_1 + L_2}{2} \cos(\theta) \sin\left(\omega_r t + \frac{2\pi n}{N}\right)\right). \tag{10}$$

Table 2 lists the parameters that were utilized in equation (10).

The distribution of random processes that increase with any type of distribution is Gaussian, according to the central limit theorem. In order to simulate the random samples of the noise mixed with the target's return signal, white Gaussian noise is assumed. The noise's power changes as the noise's variance changes. Different SNR ratios can be achieved by altering the noise power for each target independently. The signal strength at any given viewing angle is precisely equal to the signal strength for each target.

Figure 1 shows data acquisition using propeller return signal simulation using equation (10).

The components' 128-point from fast Fourier transform (FFT) are the features extracted from these signals. The feature vector of the specified SNR ratio and viewing angle (θ) is as follows:

$$\overrightarrow{feature} = [f_1.f_2.f_3. \ldots . f_{126}.f_{127}.f_{128}]_{(SNR.\theta).} \tag{11}$$

Each component corresponds to a 128-point FFT point in the SNR and the angle of view is specified. The reference targets match the 25 classes [44]. Samples of each class include feature vectors in eight viewing angles (10, 20, 30, 40, 50, 60, 70, and 80 degrees) and 9 SNRs (20, 15, 10, 5, 0, −5, −10, −15, and −s20 dB). In the specified viewing angle and SNR, 30 samples from each class with different amounts of noise are simulated. Therefore, there are 2160 samples for all viewing angles and SNRs in each class and 54,000 samples in the dataset. Figure 2 shows samples of sonar micro-Doppler signatures and simulated acoustic signals for target no. 19 at various SNRs.

3.4. Classifiers. This paper uses ensemble classifiers with weighted majority votes in addition to the separate use of popular machine learning classifiers. Independently used classifiers include k-NN, MLP-NN with the postdiffusion training algorithm, and 257 neurons in the hidden layer classifying Gaussian NB and DT. Subsection 3.4.1 describes ensemble classifiers with weighted majority votes. Subsection 3.4.1 discusses the technique of using PSO to produce the optimal weights of the classifiers.

3.4.1. Weighted Majority Vote Classifier with PSO. Ensemble learning is a method of combining predictions from various classifiers. A majority vote is one of the most effective, popular, and simplest decision fusion methods. Although majority voting may be performed in various ways, the most typical method is assigning an instance to the class with the most votes, i.e., allocating an instance to the class that most base classifiers agree on. The base classifiers in an ensemble seldom perform equally well; thus, treating them equally in aggregation may not be the best approach [50]. In this situation, weighing each classifier depending on its performance is the best strategy. The most critical challenge in weighting schemes is determining how to estimate the weights of classifiers, which can significantly impact the ensemble's performance. This paper uses PSO for the first time to generate optimal weights for classifier votes. Figure 3 shows the classification steps using the weighted majority vote and Figure 4 shows the pseudocode for the MV-PSO classifier.

The pseudocode outlines an algorithm for the MV-PSO classifier, which involves loading a dataset and defining a set of basic classifiers, including k-NN, NB, DT, MLP-NN, RF, and SVM. These classifiers form the ensemble and contribute to the final predictions.

The PSO parameters are then initialized, including the number of particles, maximum iterations, and the weights for inertia, cognitive, and social factors. These parameters control the behavior of the particle swarm optimization algorithm, which aims to optimize the weights and thresholds of the ensemble classifiers.

Then, a fitness function is defined for the PSO algorithm. This function takes inputs such as the particle (containing weights and thresholds), the dataset (X), the corresponding labels (y), the number of neighbors for k-NN (k), and instances of the basic classifiers. This function calculates the weights and thresholds from the particle and applies a majority voting scheme on the dataset using these optimized values. The resulting ensemble prediction is evaluated by comparing it to the true labels, and the correct recognition rate (accuracy) is calculated and returned.

The particles, velocities, personal best (p^{Best}), and global best (g^{Best}) arrays are then initialized to store the solutions during the PSO optimization process. The PSO algorithm runs for the specified number of maximum iterations. For

Table 2: Parameters of equation (10).

$s_r(t)$	Return signal in time
N	Number of blades
A_r	A scale factor
L_1	Distance of the blade roots from the center of rotation
L_2	Distance of the blade tips from the center of rotation
ω_c	Radian frequency of the transmitted signal
λ	The wavelength of the transmitted signal
R	Range of the center of rotation
v	The radial velocity of the center of rotation with respect to the sonar
θ	The angle between the plane of rotation and the line of sight from the sonar to the center of rotation
ω_r	Radian frequency of rotation

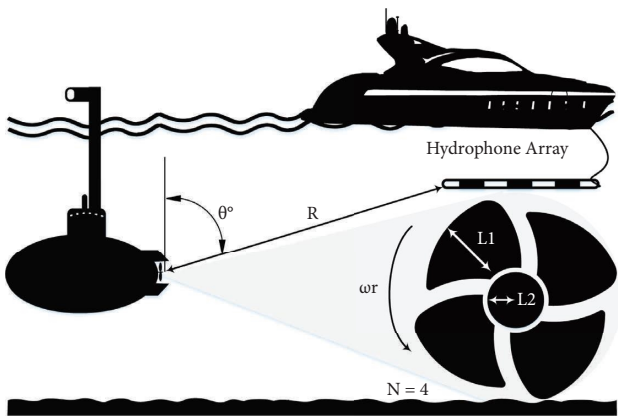

Figure 1: Data acquisition using propeller return signal simulation using equation (10).

each particle, the algorithm updates the velocity using the PSO equation and then updates the particle's position by adding the velocity. Boundaries are applied to the particle values to ensure that the weights remain within the range of [0–1]. The fitness function is evaluated for each particle, and the personal best and global best solutions are updated accordingly. This process iterates until the maximum number of iterations is reached, with the best fitness value displayed at each iteration.

After the PSO algorithm completes, the global best solution (g^{Best}) is used to evaluate the MV-PSO classifier on the entire dataset. The majority voting scheme is applied once again using the optimized weights and thresholds obtained from g^{Best}, resulting in the predicted labels of the MV-PSO classifier.

The pseudocode also includes a helper function called "evaluateClassifier." This function takes the particle, the dataset (X), the corresponding labels (y), the number of neighbors for k-NN (k), and instances of the basic classifiers as inputs. Within the function, the weights and thresholds are extracted from the particle. Each basic classifier is then applied to the dataset and the predictions are stored. The majority voting scheme is applied to these predictions using the weights and thresholds, and the ensemble prediction is obtained. The correct recognition rate is calculated by comparing the ensemble prediction with the true labels, and it is returned as the fitness value.

In summary, the pseudocode presents a detailed algorithm for the MV-PSO classifier. It encompasses the initialization of PSO parameters, the definition of a fitness function based on the correct recognition rate, the execution of the PSO optimization process, and the evaluation of the MV-PSO classifier using the optimized weights and thresholds. The algorithm utilizes the ensemble of basic classifiers and the PSO optimization to enhance the classification correct recognition rate.

Table 3 shows the PSO adjustment parameters.

For example, the initial population is assumed to consist of 16 particles and the weight vector length equals 14. Figure 5 shows how to weigh the classifiers participating in the majority voting.

The condition for stopping is to reach the correct detection rate of 100% or the maximum number of iterations. The data in the best weighting pattern are then used to classify with the MV-PSO.

4. Experimental Result and Discussion

The measured indicators in this part are presented in Subsection 4.1. Then, in the second step, the performance of STR_MD is evaluated in two phases. Therefore, the first phase, discussed in Subsection 4.2, examines the simulation results for the simulated unknown targets. The second phase, presented in Subsection 4.3, evaluates the performance of STR_MD using a dataset of practical data collected from the cavitation tunnel at different RPMs. Due to the unavailability of sonar datasets used in related articles, in Section 4.4, in order to make a comparative comparison for the MV-PSO classifier, the Gorman and Sejnowski benchmark datasets are used.

The evaluation was conducted in MATLAB-R2020a on a PC with Intel Core i7-2630QM, a 2 GHz processor, and a 6 GB RAM running memory in Windows 7.

4.1. Comparative Parameters. Measurement parameters are correct recognition rate, reliability, and processing time. In pattern recognition, reliability is an essential factor to consider. In other words, reliability establishes the legitimacy of the classifier's final ruling in the presence of a pattern. A classifier may occasionally be able to recognize every pattern in a given class accurately. Nevertheless, since other classes' patterns are included in the scope of that class, the decision's dependability is lowered.

4.2. Simulation Results for Unknown Sonar Targets Generated by STR_MD. The STR_MD simulation results are investigated in this subsection. For each experiment, the classification results are based on an average of 15 runs. Each experiment has a specified target angle of view and SNR ratio. The fabrication of random noise samples is repeated 30 times due to the randomness of the noise, making the reference data in each signal as complete as possible. For each target, 20 samples are utilized to create a reference class, while another 10 samples serve as the test data (unknown targets).

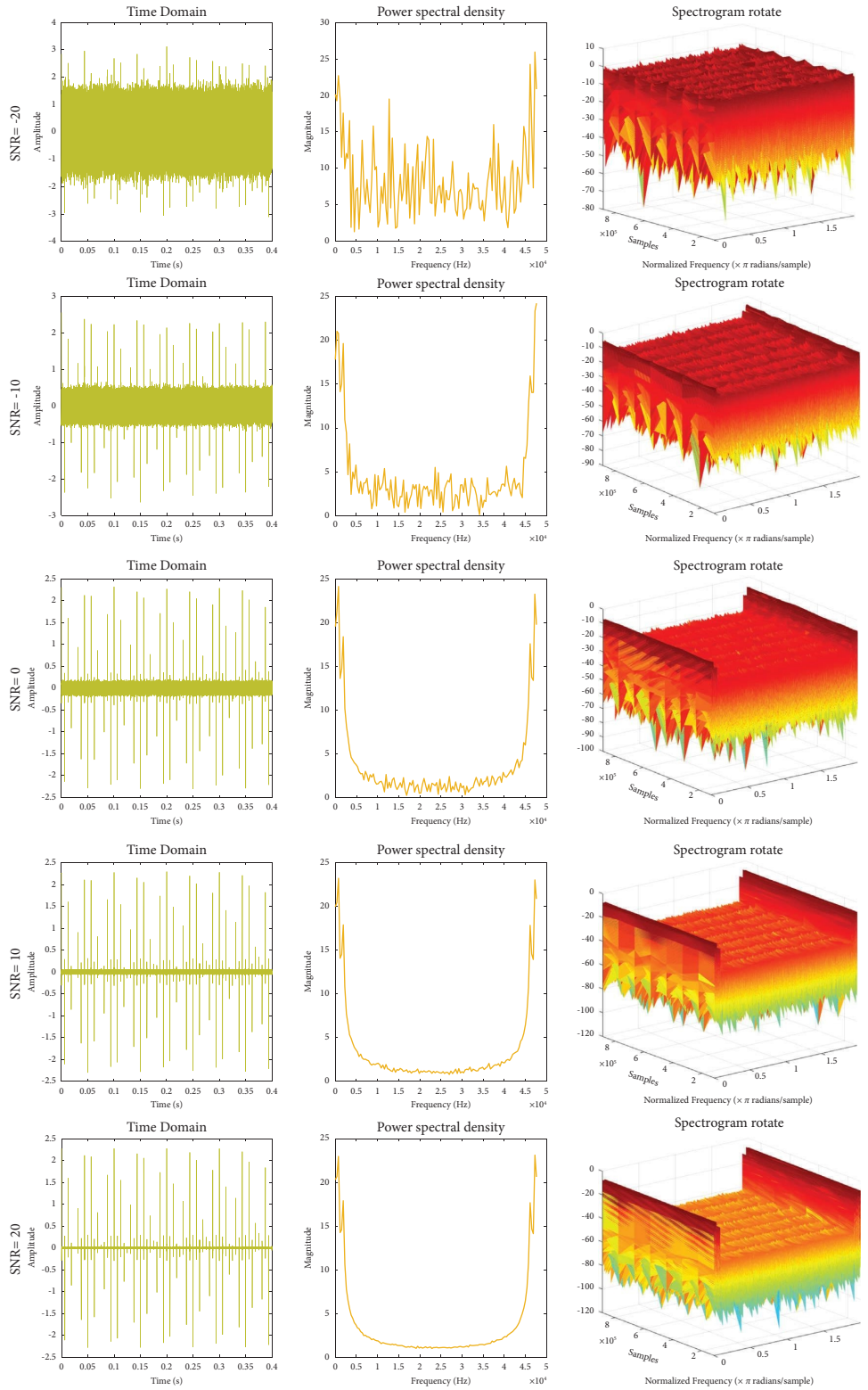

Figure 2: Samples of sonar micro-Doppler signatures and simulated acoustic signals for target no. 19 at various SNRs.

Figures 6 and 7 show the MV-PSO classifier's confusion matrix at "SNR = 15 and 40°" and "SNR = −20 and 80°," respectively.

Table 4 shows the correct recognition rate for the simulated dataset using different classifiers. For various classifiers, Figure 8 displays a correct recognition rate in

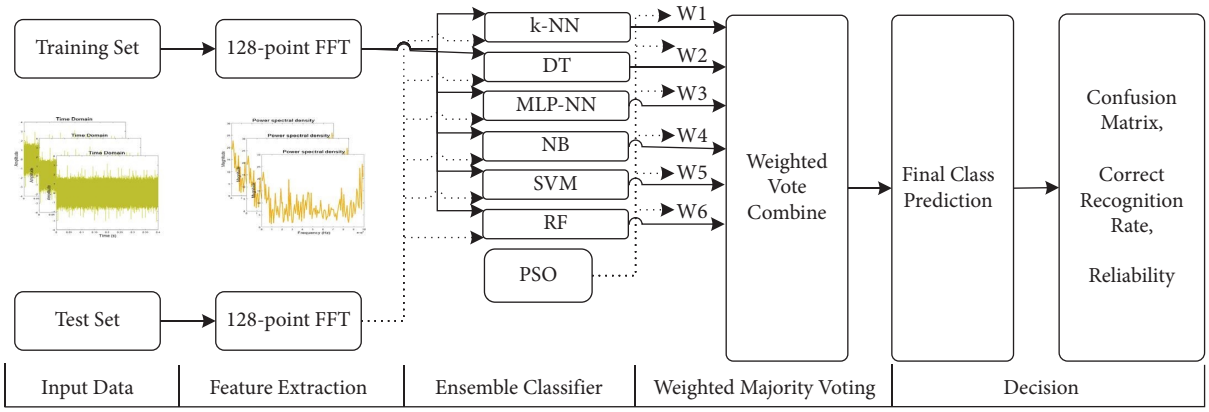

Figure 3: The classification steps use the weighted majority vote.

1. Load dataset and define basic classifiers (k-NN, NB, DT, MLP-NN, RF, SVM)
2. Initialize PSO parameters: numParticles, maxIterations, w, c1, c2
3. Define fitness function for PSO:
- Input: particle, X, y, k, nbModel, dtModel, mlpModel, rfModel, svmModel
- Calculate weights = particle[1, 3, 5, 7, 9, 11]
- Calculate thresholds = particle[2, 4, 6, 8, 10, 12]
- Apply majority voting with weights and thresholds on X
- Calculate correctRecognitionRate as the accuracy of the MV-PSO classifier
- Return correctRecognitionRate
4. Initialize particles, velocities, pBest, and gBest arrays
5. Run PSO algorithm for maxIterations:
- For each particle i in particles:
- Get particle and velocity
- Update velocity using PSO equation
- Update particle by adding velocity
- Apply boundaries to particle values (weights within [0, 1])
- Evaluate fitness function for the particle
- Update p^{Best} and g^{Best} if necessary
- Update particles and velocities arrays
- Display the best fitness value at each iteration
6. Use g^{Best} to evaluate the MV-PSO classifier on the entire dataset:
- Apply majority voting with weights and thresholds from g^{Best} on X
- Return the predicted labels of the MV-PSO classifier

```
Function evaluateClassifier(particle, X, y, k, nbModel, dtModel, mlpModel, rfModel, svmModel):
    weights = particle[1, 3, 5, 7, 9, 11]
    thresholds = particle[2, 4, 6, 8, 10, 12]
    predictions = array of zeros with shape (numSamples, numClassifiers)
    For i = 1 to numClassifiers:
        If i is k-NN:
            Apply k-NN on X with k neighbors and store predictions[:, i]
        Else if i is NB:
            Apply NB on X and store predictions[:, i]
        Else if i is DT:
            Apply DT on X and store predictions[:, i]
        Else if i is MLP-NN:
            Apply MLP-NN on X and store predictions[:, i]
        Else if i is RF:
            Apply RF on X and store predictions[:, i]
        Else if i is SVM:
            Apply SVM on X and store predictions[:, i]
    Apply majority voting with weights and thresholds on predictions and store ensemblePrediction
```

Figure 4: Pseudocode for the MV-PSO classifier.

Table 3: PSO adjustment parameters.

Parameter	Value
Population size	16
ω	0.4
$c1$	2
$c2$	2
Maximum number of iterations	50

Input Data in Run 1	Particle	k-NN	NB	DT	MLP-NN	SVM	RF
	1	85.45	43.32	90.24	28.44	93.55	18.97
	2	84.25	56.97	84.32	24.71	84.65	27.14
	⋮	⋮	⋮	⋮	⋮	⋮	⋮
	15	83.44	49.01	88.34	25.33	89.97	33.64
	16	89.45	14.26	90.97	19.87	91.51	25.68

After 50 runs

Optimal pattern for weighting (Based on g^{best})	w_1	w_2	w_3	w_4	w_5	w_6
	0.95	0.12	1	0.43	1	0.70

Voting based on the Optimal weighting pattern for an unknown target	w_1 *k-NN	w_2 *NB	w_3 *DT	w_4 *MLP-NN	w_5 *SVM	w_6 *RF
	0.95*89.45	0.12*44.35	1*90.25	0.43*22.34	1*92.25	0.70*29.65

Figure 5: How to weigh the classifiers participating in the majority voting.

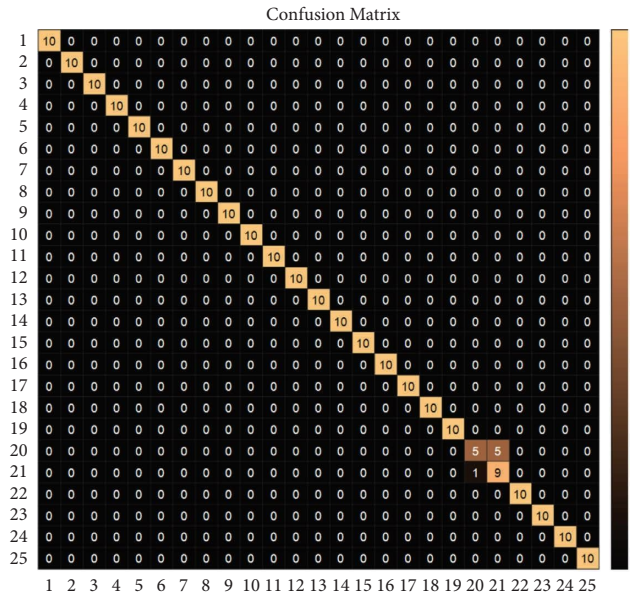

Figure 6: The confusion matrix for the MV-PSO classifier is at SNR = 15 and 40°.

terms of viewing angle at SNR = 20 dB and Figure 9 displays a correct SNR at 50° viewing angle. Figure 10 depicts the reliability rate for SNR at 20 dB for various classifiers in terms of viewing angle and Figure 11 depicts the reliability rate for SNR at 50° for various classifiers. Figure 12 illustrates the simulated dataset's correct recognition rate, MV-PSO classifier in all SNRs, and viewing angles. The reliability rate for the MV-PSO classifier is illustrated in Figure 13 for all

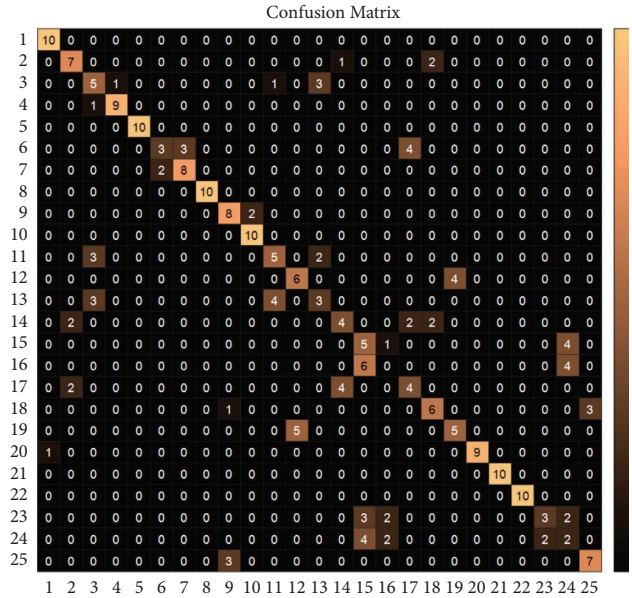

Figure 7: The confusion matrix for the MV-PSO classifier is at SNR = −20 and 80°.

Table 4: Correct recognition rate using different classifiers for the simulated dataset.

SNR (dB)	Classifier	10°	20°	30°	40°	50°	60°	70°	80°	AVR
	k-NN	95.90	96.00	96.80	95.20	94.40	95.60	95.20	95.20	95.50
	NB	95.60	96.80	96.40	95.20	94.30	95.20	95.60	96.00	95.55
	DT	96.00	95.60	95.60	94.40	97.10	96.30	94.80	96.00	95.80
20	MLP-NN	22.40	23.60	25.70	24.10	21.30	17.50	15.20	14.40	20.52
	SVM	95.60	95.80	96.00	95.80	96.00	95.60	95.60	95.20	95.67
	RF	96.10	96.00	96.60	94.59	97.20	96.70	95.20	95.00	95.91
	MV-PSO	96.59	97.80	97.20	97.59	97.50	96.90	96.90	96.59	**96.73**
	k-NN	96.40	95.20	96.00	97.60	95.20	96.00	95.20	96.80	96.05
	NB	95.20	96.00	96.40	94.00	96.40	97.60	95.60	96.80	96.00
	DT	94.40	93.60	94.40	97.60	95.20	94.00	95.60	95.20	95.00
15	MLP-NN	19.20	20.00	19.60	16.90	17.20	16.70	17.20	15.40	17.77
	SVM	96.20	94.80	96.00	96.00	96.00	96.80	95.20	96.40	95.92
	RF	94.40	93.60	94.40	97.60	95.20	94.00	95.60	95.20	95.00
	MV-PSO	96.79	96.00	96.40	97.59	96.79	97.59	97.20	97.20	**96.94**
	k-NN	95.60	94.80	95.20	96.40	96.20	97.60	96.00	96.80	96.10
	NB	96.00	94.80	94.80	96.40	95.60	96.40	96.40	96.80	95.90
	DT	94.80	94.00	95.20	94.80	94.80	95.60	96.80	96.80	95.35
10	MLP-NN	20.00	19.80	18.70	18.80	17.00	16.70	16.70	16.20	17.98
	SVM	96.00	95.59	96.00	95.59	96.00	96.39	94.00	95.60	95.64
	RF	95.80	95.59	95.59	95.80	95.80	95.60	95.59	96.10	95.73
	MV-PSO	96.10	95.79	95.59	96.59	97.10	96.80	96.59	96.40	**96.24**
	k-NN	97.20	95.20	94.00	95.60	96.40	96.00	96.40	95.60	95.80
	NB	97.60	96.00	95.20	94.40	97.00	95.20	96.00	95.20	95.85
	DT	95.60	96.00	94.40	94.80	93.60	94.80	96.00	94.80	95.50
5	MLP-NN	22.20	22.40	22.60	21.90	21.50	20.80	19.70	18.80	21.23
	SVM	95.19	96.00	96.00	97.59	94.79	95.19	96.39	96.00	95.89
	RF	95.80	96.10	95.40	95.80	95.59	95.80	96.10	95.80	95.79
	MV-PSO	98.50	96.80	95.60	96.59	97.20	95.40	96.59	96.80	**96.68**
	k-NN	94.90	95.20	95.60	95.60	96.20	96.40	95.20	92.40	95.31
	NB	95.20	96.40	94.80	95.30	96.00	95.80	95.00	91.20	94.96
	DT	93.90	94.80	96.40	96.00	94.80	93.60	95.10	90.00	94.32
0	MLP-NN	21.00	21.70	22.30	24.00	23.40	22.00	20.10	19.00	21.68
	SVM	94.79	94.79	96.79	96.00	95.59	96.39	95.00	94.00	95.41
	RF	94.90	95.80	96.59	96.10	95.80	93.59	95.40	90.20	94.79
	MV-PSO	96.10	96.59	96.80	96.89	96.89	96.80	96.50	95.40	**96.49**

Table 4: Continued.

SNR (dB)	Classifier	10°	20°	30°	40°	50°	60°	70°	80°	AVR
	k-NN	94.80	96.80	95.20	92.00	94.00	94.00	94.40	90.80	94.00
	NB	95.60	96.40	94.80	95.20	94.40	94.40	96.00	88.80	94.45
	DT	94.40	92.00	93.20	94.00	93.20	91.20	94.00	92.00	93.00
−5	MLP-NN	16.00	16.90	17.00	16.20	15.70	15.30	14.80	14.10	15.75
	SVM	95.00	96.70	95.59	94.34	94.39	94.00	94.79	91.20	94.50
	RF	94.59	92.10	93.80	94.59	93.40	91.10	94.10	92.20	93.23
	MV-PSO	95.70	97.59	97.40	95.59	95.80	94.59	96.10	92.60	**95.67**
	k-NN	88.00	88.80	88.80	90.40	87.20	87.60	84.80	75.60	86.40
	NB	90.40	89.60	89.60	86.40	87.60	86.00	81.20	82.40	86.65
	DT	82.40	82.80	88.40	87.20	85.60	87.20	87.20	75.60	84.55
−10	MLP-NN	15.90	15.80	15.90	15.00	14.60	13.20	13.10	12.30	14.47
	SVM	89.20	87.20	90.00	90.00	86.79	87.20	88.79	84.39	87.94
	RF	84.59	84.80	88.59	87.40	86.60	87.59	87.40	75.59	85.32
	MV-PSO	90.59	90.10	90.80	88.80	88.59	87.40	87.40	82.59	**88.28**
	k-NN	80.80	78.40	78.00	83.20	78.40	72.40	74.40	64.40	76.25
	NB	84.80	84.40	81.20	82.00	80.00	74.40	74.40	69.20	78.80
	DT	81.20	82.80	73.60	75.20	77.60	78.00	75.60	63.20	75.90
−15	MLP-NN	14.60	14.80	14.70	14.10	13.40	12.00	11.70	11.20	13.31
	SVM	83.20	77.28	77.59	83.00	78.59	71.10	74.00	65.59	76.29
	RF	81.59	82.59	73.59	75.10	77.59	78.10	75.10	63.40	75.88
	MV-PSO	84.80	84.80	81.40	84.40	80.20	78.10	76.20	70.79	**80.08**
	k-NN	66.80	66.00	64.40	66.80	68.40	66.40	59.60	50.40	63.60
	NB	67.60	68.80	64.00	69.20	66.40	65.60	63.20	54.00	64.85
	DT	76.00	78.80	74.00	76.00	73.60	74.80	70.00	63.60	73.35
−20	MLP-NN	11.80	12.00	12.70	12.50	11.80	10.40	9.50	8.00	11.08
	SVM	69.60	69.60	67.40	68.20	67.59	67.00	61.59	53.10	65.51
	RF	76.10	78.60	74.00	76.00	73.59	74.60	69.80	63.20	73.23
	MV-PSO	76.20	78.80	74.20	76.79	74.79	74.79	70.20	63.60	**73.67**

Bold values are actually the best answers (highest recognition rate).

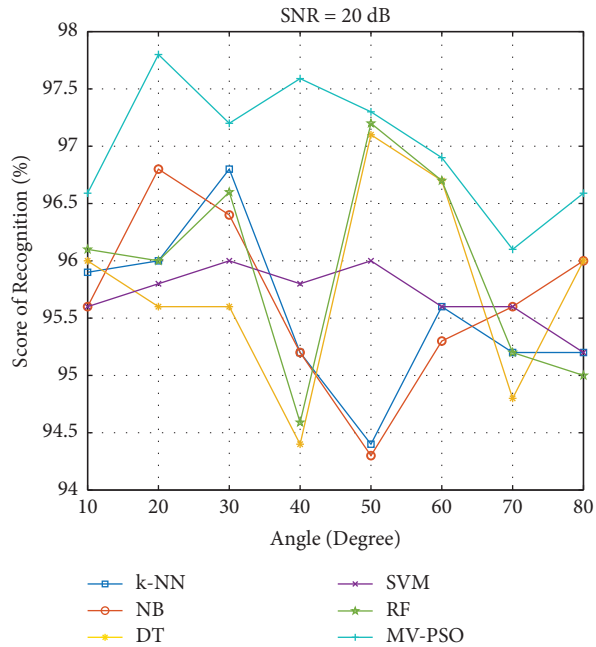

Figure 8: Correct recognition rate in terms of viewing angle at SNR = 20 dB for different classifiers.

SNRs and viewing angles of the simulated dataset. Table 5 shows the reliability rate of different classifiers in the simulated dataset classification.

In general, the simulation results show that the k-NN, NB, SVM, RF, and DT classifiers perform encouragingly in terms of correct recognition and reliability. As shown in

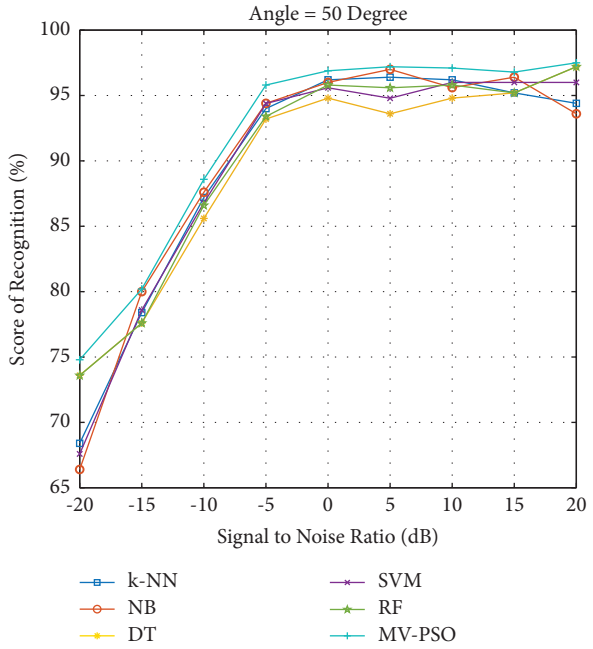

Figure 9: Correct recognition rate in terms of SNR at 50° viewing angle for different classifiers.

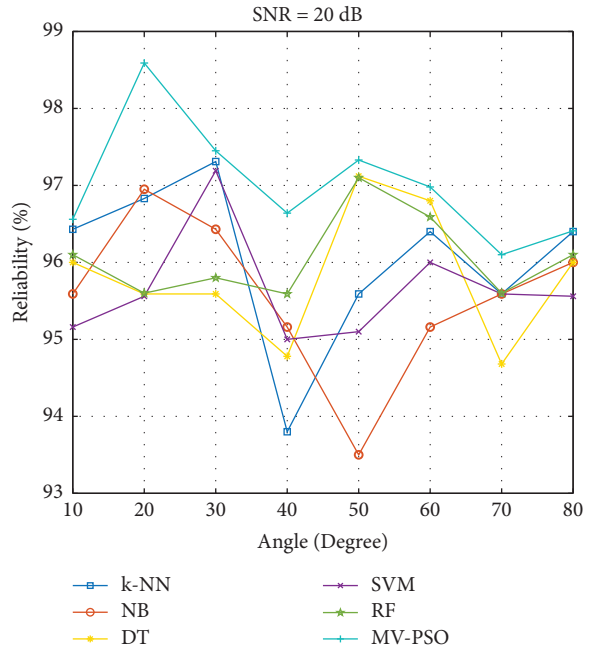

Figure 10: Reliability rate in terms of viewing angle at SNR = 20 dB for different classifiers.

Tables 4 and 5, in positive SNRs, the performance of k-NN, NB, and SVM is almost better than that of other classifiers and MLP-NN has the weakest performance. With the addition of noise, DT and RF show their ability, so that at SNR = −20 dB, we see better performance of RF than other classifiers. However, the MV-PSO classifier, which uses the weighted votes of the base classifiers, shows better results than the base classifiers in all SNRs in terms of correct recognition rate and reliability.

Table 6 shows the decision time for an unknown target. Obviously, processing time plays a vital role in identifying anonymous samples in the automatic sonar target recognition system. The shortest time is related to the k-NN classifier.

The MV-PSO classifier proposed in the paper exhibits a number of advantages and disadvantages when compared to the other classifiers used in the study. First, one of the notable advantages of MV-PSO is its ability to achieve an

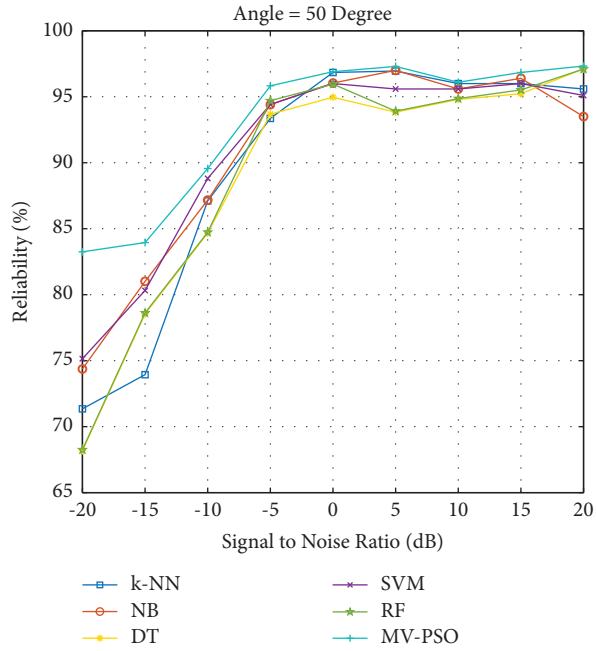

Figure 11: Reliability rate in terms of SNR at 50° viewing angle for different classifiers.

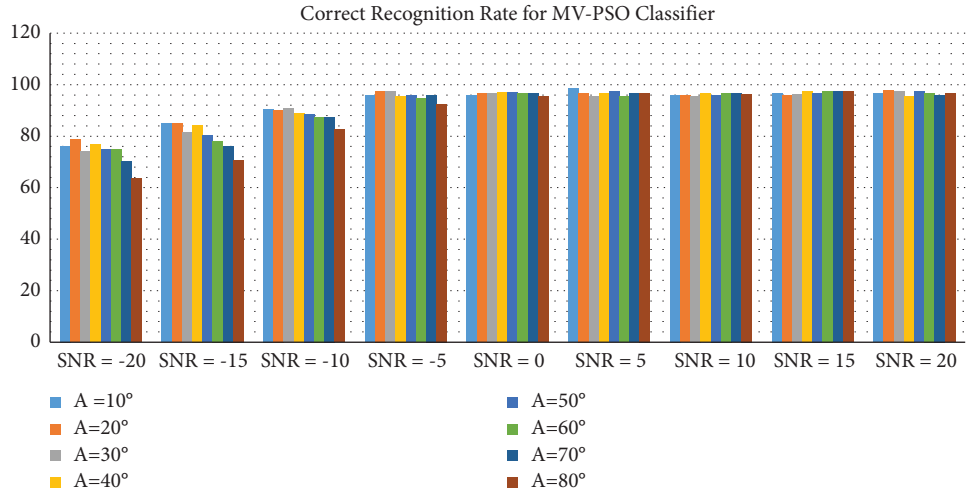

Figure 12: Correct recognition rate, MV-PSO classifier in all viewing angles, and SNRs of the simulated dataset.

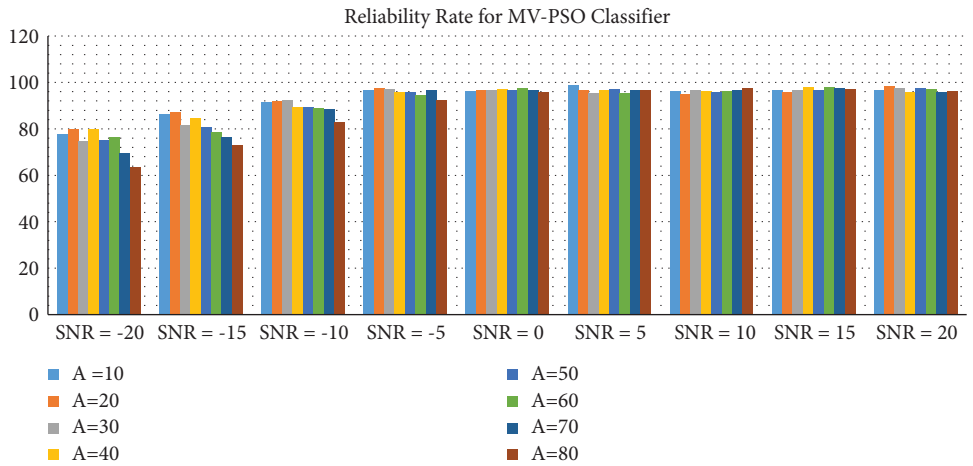

Figure 13: Reliability rate, MV-PSO classifier in all SNRs, and viewing angles of the simulated dataset.

Table 5: Reliability rate of different classifiers in the simulated dataset classification.

SNR (dB)	Classifier	10°	20°	30°	40°	50°	60°	70°	80°	AVR
	k-NN	96.43	96.83	97.31	93.80	95.59	96.40	95.59	96.40	96.04
	NB	95.59	96.95	96.43	95.16	93.50	95.16	95.59	96.00	95.54
	DT	96.00	95.59	95.59	94.78	97.12	96.80	94.68	96.00	95.82
20	MLP-NN	21.33	21.50	23.06	21.46	21.30	19.00	17.99	14.33	19.99
	SVM	95.16	95.56	97.19	96.00	95.10	96.00	95.59	95.56	95.77
	RF	96.10	95.60	95.80	95.59	97.10	96.59	95.60	96.10	96.06
	MV-PSO	96.56	98.59	97.45	95.64	97.33	96.98	96.10	96.41	**96.88**
	k-NN	96.80	96.00	95.16	96.80	96.00	96.00	96.83	96.53	96.26
	NB	95.16	96.00	96.40	93.80	96.40	97.90	95.56	96.80	96.00
	DT	94.47	93.55	94.31	97.90	95.23	93.80	95.63	95.20	95.01
15	MLP-NN	19.58	19.00	19.33	17.70	17.23	15.88	17.41	14.11	17.53
	SVM	96.43	95.20	96.80	96.00	96.00	96.00	94.68	97.21	96.04
	RF	94.51	93.59	94.64	97.93	95.52	93.80	95.79	95.33	95.13
	MV-PSO	96.83	96.10	96.50	97.91	96.84	97.93	97.59	97.25	**97.11**
	k-NN	95.56	94.40	95.59	95.20	96.00	96.00	95.16	96.83	95.59
	NB	96.00	94.68	94.68	96.40	95.59	96.43	96.43	96.95	95.89
	DT	94.68	93.80	95.16	94.78	94.80	95.59	96.80	96.83	95.30
10	MLP-NN	19.78	19.98	18.53	16.25	16.47	16.77	15.10	13.59	17.05
	SVM	95.59	93.80	96.40	96.00	95.59	96.00	95.59	96.00	95.62
	RF	95.59	93.70	95.16	94.91	94.86	95.68	96.89	96.94	95.46
	MV-PSO	96.21	94.79	96.63	96.40	96.10	96.43	96.53	97.72	**96.35**
	k-NN	97.21	96.00	93.60	96.43	96.95	94.75	96.78	96.83	96.06
	NB	97.66	96.00	95.20	94.40	97.00	95.20	96.00	95.16	95.85
	DT	95.95	96.56	94.03	94.68	93.83	94.68	96.00	94.83	95.07
5	MLP-NN	21.21	20.33	20.33	20.59	20.63	19.78	19.24	16.19	19.78
	SVM	98.02	96.39	96.40	96.00	95.59	96.00	95.59	96.00	96.24
	RF	95.97	96.59	94.19	94.73	93.91	94.70	96.10	94.85	95.13
	MV-PSO	98.89	96.50	95.21	96.50	97.30	95.30	96.79	96.86	**96.66**
	k-NN	96.04	95.16	95.59	95.19	96.84	96.53	96.40	92.59	95.54
	NB	95.16	96.43	94.68	95.73	96.04	96.00	95.16	95.48	95.58
	DT	94.94	95.07	96.43	96.00	94.96	93.58	95.59	92.06	94.82
0	MLP-NN	20.54	20.11	22.33	22.08	21.74	21.80	21.83	18.10	21.06
	SVM	96.00	96.00	96.43	95.53	96.00	96.83	94.78	94.79	95.79
	RF	94.98	96.07	96.20	96.10	95.96	94.58	95.80	92.60	95.28
	MV-PSO	96.40	96.59	96.59	96.95	96.90	97.32	96.50	95.67	**96.60**
	k-NN	94.75	97.66	97.21	94.20	93.36	94.01	95.27	91.89	94.79
	NB	95.59	96.40	94.78	95.20	94.40	94.31	96.04	88.89	94.45
	DT	94.70	91.87	93.51	94.23	93.68	91.08	94.24	92.45	93.22
−5	MLP-NN	15.12	16.59	14.07	15.47	15.31	15.33	12.82	14.12	14.85
	SVM	96.00	96.95	95.59	94.24	94.42	94.01	94.86	91.23	94.66
	RF	95.70	95.88	94.51	95.33	94.70	94.10	94.53	92.65	94.67
	MV-PSO	96.59	97.66	97.30	95.71	95.83	94.42	96.49	92.49	**95.81**
	k-NN	85.71	91.00	89.28	88.56	87.11	82.47	83.48	76.66	85.53
	NB	90.48	89.65	89.52	86.95	87.17	87.02	81.48	82.80	86.88
	DT	82.86	82.72	88.44	86.90	84.67	87.94	87.23	76.20	84.62
−10	MLP-NN	16.99	15.28	16.59	15.50	14.18	13.00	13.27	11.10	14.48
	SVM	89.17	87.11	90.27	90.26	88.81	87.93	89.27	84.54	88.42
	RF	82.91	82.98	88.50	86.99	84.73	87.95	87.33	76.38	84.72
	MV-PSO	91.48	92.00	92.28	89.56	89.56	88.92	88.37	82.90	**89.38**
	k-NN	81.54	80.51	77.03	84.69	73.94	71.05	74.15	71.36	76.78
	NB	86.06	84.63	81.65	82.25	81.01	73.81	74.82	68.88	79.13
	DT	81.57	83.82	75.02	75.55	78.54	78.52	75.85	63.09	76.49
−15	MLP-NN	13.22	16.58	14.33	14.33	13.10	11.28	11.77	10.20	13.10
	SVM	84.93	86.94	83.80	83.65	80.32	79.54	84.58	76.09	82.85
	RF	82.66	83.88	75.30	75.65	78.62	78.64	75.91	63.64	76.78
	MV-PSO	86.41	87.25	81.71	84.73	83.95	78.66	76.63	72.82	**81.14**

Table 5: Continued.

SNR (dB)	Classifier	10°	20°	30°	40°	50°	60°	70°	80°	AVR
	k-NN	63.83	72.62	65.68	67.56	71.35	63.85	56.50	51.35	64.09
	NB	77.66	79.77	74.57	77.92	74.37	76.55	69.53	63.41	74.22
	DT	68.03	68.53	64.39	72.41	68.18	65.29	65.04	54.12	65.74
−20	MLP-NN	11.23	11.01	11.50	13.44	10.36	8.15	8.89	7.48	10.25
	SVM	81.13	79.82	77.50	81.02	75.15	81.83	73.99	74.14	79.07
	RF	68.15	68.64	64.44	72.53	68.25	65.37	65.18	54.20	65.84
	MV-PSO	77.81	79.93	74.63	79.98	83.25	76.66	69.53	63.44	**74.65**

The bold values are the best reliability rates in different classifiers and different SNRs.

Table 6: Decision time for an unknown target.

Classifier	k-NN	NB	DT	MLP-NN	SVM	RF	MV-PSO
Time (s)	**0.5148**	0.6293	0.9866	2.0616	1.04	1.03	9.81

Bold values are actually the best answers.

improved recognition rate and higher reliability than the other six classifiers. The experimental results consistently demonstrate that MV-PSO outperformed its counterparts in accurately recognizing sonar targets. This indicates that the combination of multiple classifiers and the utilization of PSO for weighted voting contribute to the enhanced performance of MV-PSO.

Another strength of MV-PSO lies in its ability to leverage the knowledge and diversity of the ensemble of basic classifiers. By combining the predictions of k-NN, NB, DT, MLP-NN, SVM, and RF, MV-PSO benefits from the collective expertise and robustness of these individual classifiers. This ensemble approach is advantageous as it helps mitigate the limitations and biases that may be present in any single classifier.

Furthermore, the adoption of PSO for weighted voting in MV-PSO is an additional strength. PSO optimizes the weights assigned to the predictions of the basic classifiers, thereby incorporating the varying importance and reliability of each classifier's output. This process improves the overall classification performance by assigning more weight to the classifiers with higher accuracy or expertise in specific areas.

On the other hand, MV-PSO exhibits disadvantages that need to be considered. One of the disadvantages of MV-PSO is the lack of transparency and interpretability. As MV-PSO combines the predictions of multiple classifiers and assigns weights through PSO, the decision-making process becomes more complex and less interpretable. This lack of transparency can hinder the ability to understand and explain the reasoning behind MV-PSO's classifications, which may be a requirement in certain applications.

Another weakness of MV-PSO is the increased processing time compared to other classifiers. The reliance on the votes of multiple classifiers and the computational complexity introduced by the PSO optimization process contribute to this longer processing time. However, despite this drawback, it is important to note that the processing time of MV-PSO remains relatively suitable and useable for real-world applications. While it may not be as fast as some other classifiers, the performance gains achieved by MV-PSO justify its practical viability, making it a promising option for real-world implementation.

In summary, the strengths of MV-PSO include its improved recognition rate, the utilization of ensemble classification, and the application of PSO for weighted voting. These strengths enhance the recognition rate and reliability of the classifier. On the other hand, the disadvantages of MV-PSO lie in the increased processing time and potential computational overhead. Nevertheless, despite the longer processing time, MV-PSO remains a practical option for real-world applications due to its overall performance and benefits.

In order to perform proper validation of the STR_MD, the practical data obtained from the cavitation tunnel is used for testing in the following subsection.

4.3. Test Practical Dataset. The focus of the STR_MD is on the signals received from the propellers of surface vessels and submarines. Four distinct propeller models were therefore placed in the cavitation tunnel test location, and sonar data were afterwards gathered using 2 hydrophones in order to validate the model with real-world data. This indicates, given that the sonar was directly acquired from the target propeller, that there is a micro-Doppler effect in the captured signal.

The NA-10 England cavitation tunnel has been used to generate and collect reliable sonar data. In this experiment, four propellers with different dimensions and specifications were used. The parameters of each propeller are shown in Table 7. This test's propeller revolution rate is 60, 600, 1200, 1800, 2400, and 2940 RPM and flow speeds are 4.5 m/s.

Sonar has been collected in the cavitation tunnel using two B&K 8103-type hydrophones. The data accusation board type UDAQ Lite is connected to the hydrophones.

Figure 14 shows samples of signals obtained in the cavitation tunnel by various propellers at 60 RPM.

Figure 15 shows the confusion matrix's MV-PSO classifier for the practical test dataset at 60 RPM and Figure 16 shows the confusion matrix's MV-PSO classifier for the practical test dataset at 2940 RPM. Table 8 shows the result of the recognition using different classifiers for the practical dataset. Figure 17 shows the correct recognition rate for the practical test dataset with different classifiers in all RPMs. Figure 18 shows the reliability rate for the practical test dataset with different classifiers in all RPMs.

Table 7: The parameters of each propeller.

Name	Number of blades	Full-scale diameter (m) (mm)	AE/AO	P/D	T0	J
A	3	74	0.560	0.50	1.40	0.64
B	4	91	0.665	0.90	1.40	0.75
C	5	128	0.870	1.1	1.40	0.93
D	6	134	0.905	1.25	1.40	0.99

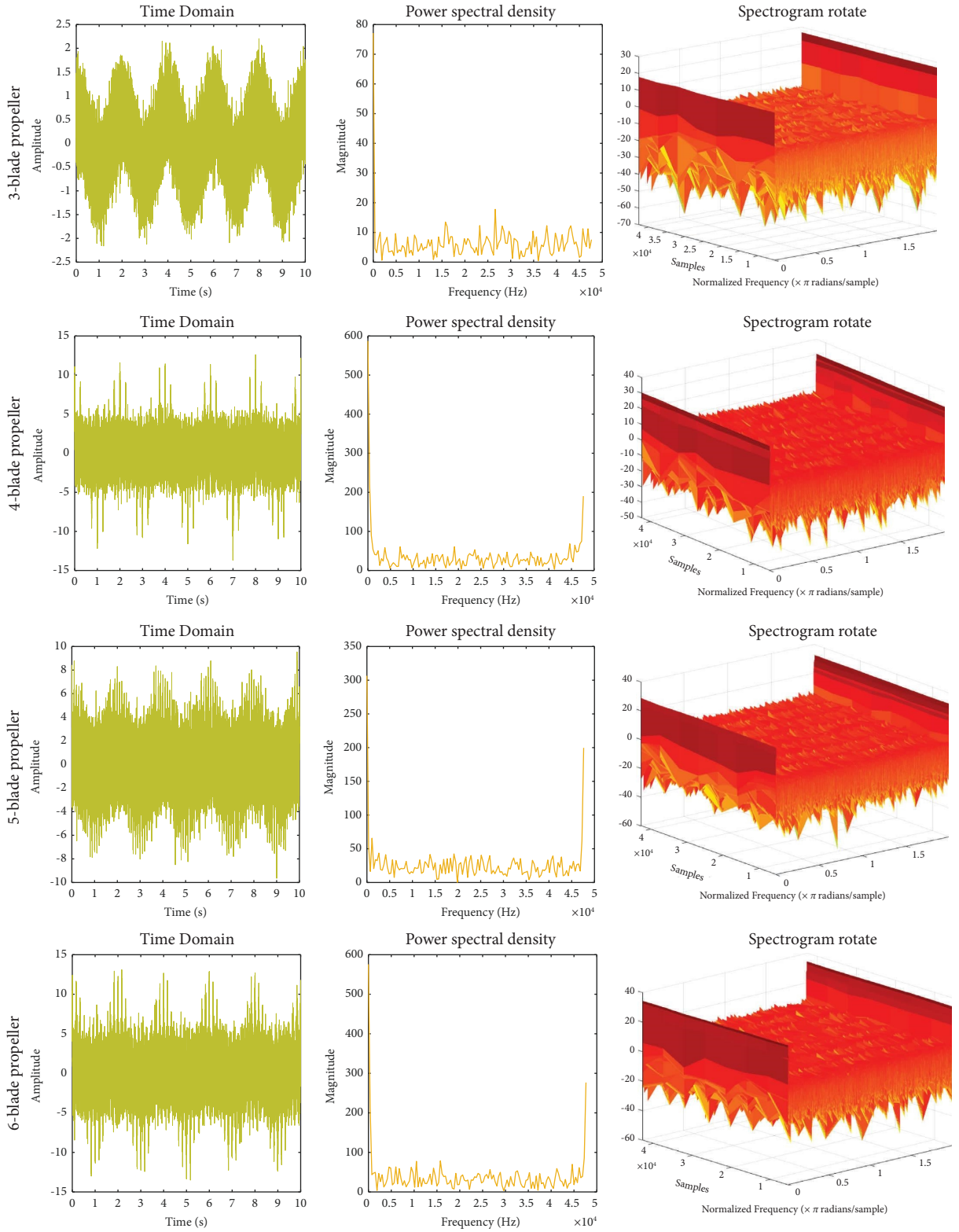

Figure 14: Samples of signals obtained in the cavitation tunnel by various propellers at 60 RPM.

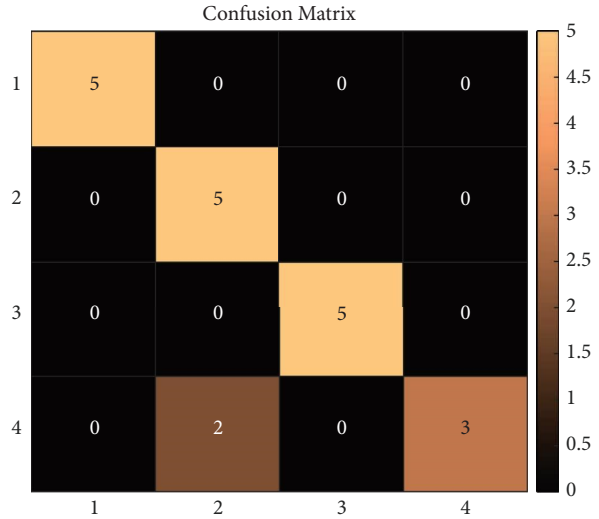

Figure 15: Confusion matrix's MV-PSO classifier for the practical test dataset at 60 RPM.

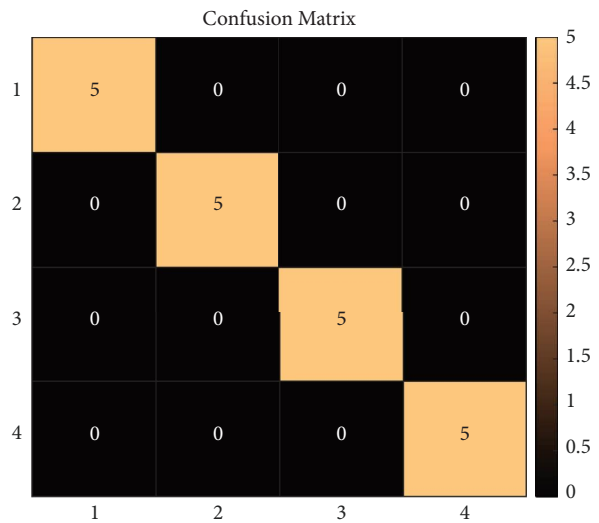

Figure 16: Confusion matrix's MV-PSO classifier for the practical test dataset at 2940 RPM.

Table 8: The result of the recognition using different classifiers for the practical dataset.

Classifier	Parameter	RPM						
		60	600	1200	1800	2400	2940	AVR
k-NN	Correct recognition rate (%)	90.00	90.62	100	100	100	100	96.77
	Reliability rate (%)	92.85	85.00	100	100	100	100	96.30
	Time (s)	0.81	0.79	0.85	0.83	0.91	0.78	0.82
NB	Correct recognition rate (%)	75.00	85.00	100	100	100	100	93.33
	Reliability rate (%)	NaN	90.62	100	100	100	100	NaN
	Time (s)	0.86	0.91	0.91	0.96	0.89	0.90	0.90
DT	Correct recognition rate (%)	80.00	70.00	100	100	60.00	70.00	80.00
	Reliability rate (%)	80.00	70.00	100	100	66.66	72.85	81.58
	Time (s)	0.84	0.82	0.89	0.81	0.94	0.78	0.84
MLP-NN	Correct recognition rate (%)	28.45	25.12	29.15	30.84	27.28	24.69	27.58
	Reliability rate (%)	23.74	36.28	28.32	30.11	31.25	27.55	29.54
	Time (s)	1.27	1.14	1.84	1.33	1.78	1.06	1.15

Table 8: Continued.

Classifier	Parameter	RPM						
		60	600	1200	1800	2400	2940	AVR
SVM	Correct recognition rate (%)	90.00	98.03	100	100	100	100	98.00
	Reliability rate (%)	92.85	99.11	100	100	100	100	98.66
	Time (s)	0.9	1.0	0.9	1.0	0.9	0.6	0.88
RF	Correct recognition rate (%)	83.00	82.00	100	100	75.00	78.00	86.33
	Reliability rate (%)	86.00	80.00	100	100	78.46	77.33	86.96
	Time (s)	0.93	0.94	0.89	0.90	0.94	0.92	0.92
MV-PSO	Correct recognition rate (%)	93.00	98.80	100	100	100	100	98.63
	Reliability rate (%)	95.93	97.30	100	100	100	100	98.87
	Time (s)	4.62	4.28	4.43	4.81	5.33	4.75	4.70

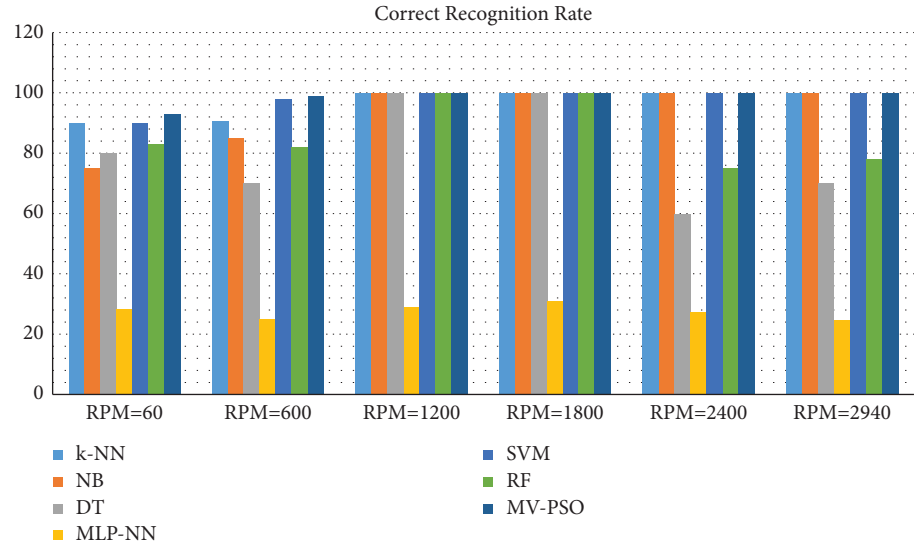

Figure 17: The correct recognition rate for the practical test dataset with different classifiers in all RPMs.

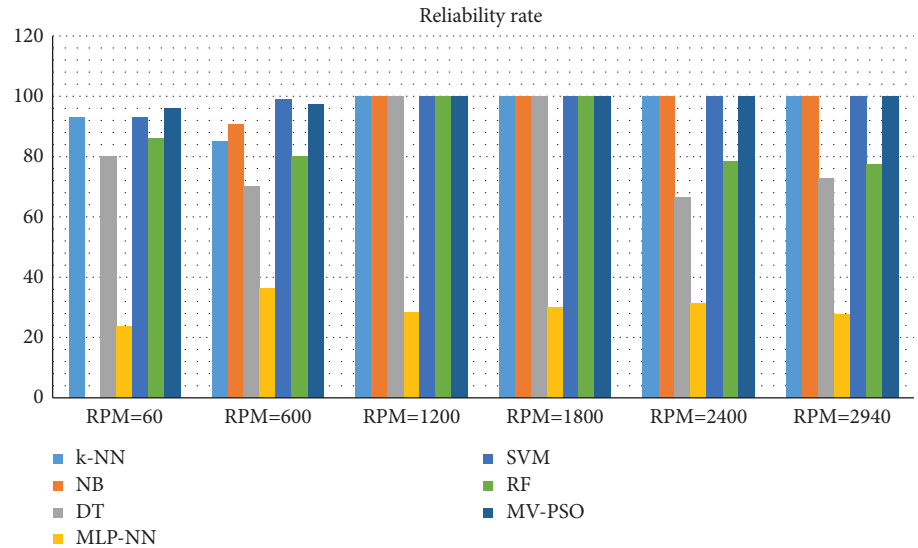

Figure 18: The reliability rate for the practical test dataset with different classifiers in all RPMs.

Table 9: The classification results of the different classifiers for the benchmark dataset.

Classifiers	k-NN	NB	DT	MLP-NN	SVM	RF	MV-PSO
Correct recognition rate	87.00	67.80	72.10	15.24	85.22	75.43	**89.57**
Reliability rate	71.25	58.89	57.61	24.74	87.41	62.28	**91.25**
Time (s)	0.01	0.01	0.01	0.41	0.03	0.01	1.31

Bold values are actually the best answers (highest recognition rate and highest reliability).

Table 10: The correct recognition rate for Gorman and Sejnowski datasets in related works.

Reference	Classifier	Correct recognition rate (%)
[56]	RBF-SCA	91.01
[61]	XGBoost	88.10
[68]	WLTSVM	87.50
[69]	Neural network + OMKL	83.00

As shown in Table 8, of the basic classifiers, the k-NN classifier performed better for real sonar data in terms of correct recognition rate, reliability rate, and processing time. Subsequently, NB had higher detection rates than DT and MLP-NN. However, the results of the MV-PSO show a more encouraging and better performance compared to the other basic classifiers used.

The MV-PSO algorithm offers practical implications and potential applications in the field of STR_MD. One significant practical implication is its potential to enhance the accuracy and reliability of target classification. Micro-Doppler signatures provide valuable motion-related information about underwater targets but analyzing these complex patterns can be challenging. By leveraging the MV-PSO's collective intelligence and majority voting mechanism, the classifier can effectively handle intricate patterns, reducing the risk of misclassification and improving overall recognition accuracy. Furthermore, the MV-PSO's ability to adapt and generalize well to different target classes makes it suitable for practical applications where targets may exhibit diverse behaviors and appearances. In addition, its optimization for efficacy harnessing the MV-PSO's capabilities, underwater surveillance, exploration, and defense applications can benefit from improved target recognition performance and autonomy in decision-making processes.

4.4. Benchmark Sonar Dataset. Since sonar datasets used in articles are often prepared in practice and are not accessible, this subsection uses Gorman and Sejnowski datasets [67] as benchmark datasets for comparative comparison with other methods. Table 9 shows the classification results of the different classifiers for this benchmark dataset. Table 10 shows the correct recognition rate for the Gorman dataset in related works.

As shown in Tables 9 and 10, the MV-PSO performed relatively well. Nevertheless, the RBF-SCA classifier performed better than the MV-PSO.

5. Conclusion

The sonar micro-Doppler signature and ensemble classifier MV-PSO are used in this paper to propose a novel technique for automatically recognizing sonar targets. Based on the return signal from the marine target propeller, the STR_MD method classifies targets in the feature space. In this approach, the various sonar targets can be recognized quickly, correctly, and reliably. The simulation results for basic classifiers indicate that k-NN classifiers, NB and DT, have significant automatic sonar target recognition performance. By measuring the processing time, it can be concluded that among the classifiers used, k-NN works better. MLP-NN performed poorly due to data volume. However, due to the use of weighted votes of the base classifiers and decision fusion in the MV-PSO ensemble classifier, this classifier has performed well for all simulated datasets SNRs and all practical datasets RPMs. Although it is necessary to research and study various machine learning solutions due to military and commercial applications as well as the novelty of the micro-Doppler signature for sonar targets located in a complex ocean and sea environment, looking at the classifiers used in this paper is recommended for the actual application of an MV-PSO classifier.

The following are under consideration for future research:

(i) Improving the performance of MLP-NN classifiers using metaheuristic algorithms

(ii) Using convolutional neural networks for automatic recognition of sonar targets

(iii) Use of hybrid classifiers to achieve more accurate accuracy for sensitive applications

(iv) Implementing MV-PSO to detect sonar targets using FPGA automatically

This paper was conducted in three general phases. The first phase collects information from different targets to model the effect of their sonar micro-Doppler. The second phase involves modeling the return signal from the sonar target propeller and extracting features from it by using the 128-point FFT. In fact, at this stage, the frequency signature or micro-Doppler effect is determined for each target. The third step deals with classification by basic machine learning classifiers and using weighted majority votes in basic classifiers.

It should be noted that the main limitation of this research is the dataset. Undoubtedly, the availability of a comprehensive dataset encompassing various categories of floats and submarines, reflective of the genuine oceanic environment, wherein all unwanted signals, comprising noise, clutter, and reverberation, would greatly enhance the overall confidence level of the research findings. However, it is important to acknowledge that executing such a test scenario incurs significant financial expenses.

Data Availability

The data used to support the findings of the study are available from the corresponding author upon request.

Conflicts of Interest

The authors declare that they have no conflicts of interest or personal relationships that could have appeared to influence the work reported in this paper.

Acknowledgments

This study was supported via funding from Prince Sattam bin Abdulaziz University project number (PSAU/2023/R/1445). The researchers would like to acknowledge Deanship of Scientific Research, Taif University for funding this work.

References

[1] E. Chen and J. Guo, "Real time map generation using sidescan sonar scanlines for unmanned underwater vehicles," *Ocean Engineering*, vol. 91, pp. 252–262, 2014.

[2] J. Tan, H. Jin, H. Hu, R. Hu, H. Zhang, and H. Zhang, "WF-MTD: evolutionary decision method for moving target defense based on wright-Fisher process," *IEEE Transactions on Dependable and Secure Computing*, vol. 15, pp. 1–14, 2022.

[3] N. Korany, "Application of wavelet transform for classification of underwater acoustic signals," *Proceedings of Meetings on Acoustics*, vol. 28, 2018.

[4] L. Qian, Y. Zheng, L. Li, Y. Ma, C. Zhou, and D. Zhang, "A new method of inland water ship trajectory prediction based on long short-term memory network optimized by genetic algorithm," *Applied Sciences*, vol. 12, no. 8, p. 4073, 2022.

[5] C. Ding, C. Li, Z. Xiong, Z. Li, and Q. Liang, "Intelligent identification of moving trajectory of autonomous vehicle based on friction nano-generator," *IEEE Transactions on Intelligent Transportation Systems*, vol. 12, pp. 1–8, 2023.

[6] T. Plessas, "Optimization of ship design for life cycle operation with uncertainties," in *Proceedings of the 13th International Marine Design Conference (IMDC 2018)*, Helsinki, Finland, June 2018.

[7] X. Liang, Z. Huang, S. Yang, and L. Qiu, "Device-free motion & trajectory detection via RFID," *ACM Transactions on Embedded Computing Systems*, vol. 17, no. 4, pp. 1–27, 2018.

[8] G. Zhou, R. Zhang, and S. Huang, "Generalized buffering algorithm," *IEEE Access*, vol. 9, pp. 27140–27157, 2021.

[9] J. Binner, J. Becktor, E. Boukas, M. Blanke, and L. Nalpantidis, "Reweighting neural network examples for robust object detection at sea Reweighting neural network examples for robust object detection at sea," *Electronics Letters*, vol. 53, pp. 19–22, 2021.

[10] A. Papanikolaou, Y. Xing-kaeding, J. Strobel, and A. Kanellopoulou, "Numerical and experimental optimization study on a fast," *Journal of Marine Science and Engineering*, vol. 8, 2020.

[11] W. Qiao, M. Khishe, and S. Ravakhah, "Underwater targets classification using local wavelet acoustic pattern and Multi-Layer Perceptron neural network optimized by modified Whale Optimization Algorithm," *Ocean Engineering*, vol. 219, Article ID 108415, June 2020.

[12] M. Blanke and L. Nalpantidis, "Vision-based object tracking in marine environments using features from neural network detections vision-based object tracking in marine environments using features from neural network detections," *IFAC-Papers On Line*, vol. 53, 2020.

[13] J. D. Stets and F. E. T. Sch, "Comparing spectral bands for object detection at sea using convolutional neural networks comparing spectral bands for object detection at sea using convolutional neural networks," *Journal of Physics: Conference Series*, vol. 1357, 2019.

[14] M. Khishe and H. Mohammadi, "Passive sonar target classi fi cation using multi-layer perceptron trained by salp swarm algorithm," *Ocean Engineering*, vol. 181, pp. 98–108, 2019.

[15] L. Carral, J. Lara-Rey, L. Castro-Santos, and J. Carral Couce, "Oceanographic research vessels: de fi ning scienti fi c winches for fi sheries science biological sampling manoeuvres," *Ocean Engineering*, vol. 154, pp. 121–132, 2017.

[16] M. R. Mosavi and M. Khishe, "Training a feed-forward neural network using particle swarm optimizer with autonomous groups for sonar target classification," *Journal of Circuits, Systems, and Computers*, vol. 26, pp. 1750185–1750211, 2017.

[17] N. Hurtós, N. Palomeras, A. Carrera, and M. Carreras, "Autonomous detection, following and mapping of an underwater chain using sonar," *Ocean Engineering*, vol. 130, pp. 336–350, 2017.

[18] H. Wang, X. Zhang, and S. Jiang, "A laboratory and field universal estimation method for tire–pavement interaction noise (TPIN) based on 3D image technology," *Sustainability*, vol. 14, pp. 12066–12119, 2022.

[19] M. Najafzadeh and F. Saberi-movahed, "GMDH-GEP to predict free span expansion rates below pipelines under waves," *Marine Georesources & Geotechnology*, vol. 37, no. 3, pp. 375–392, 2018.

[20] M. Najafzadeh, F. S. Movahed, and S. Sarkamaryan, "Nf-gmdh based self-organized systems to predict bridge pier scour depth under debris flow effects nf-gmdh based self-organized systems to predict bridge pier scour depth under debris flow effects," *Marine Georesources & Geotechnology*, vol. 36, 2017.

[21] S. Lu, Y. Ding, M. Liu, Z. Yin, L. Yin, and W. Zheng, "Multiscale feature extraction and fusion of image and text in vqa," *International Journal of Computational Intelligence Systems*, vol. 6, 2023.

[22] A. S. Mahboob and S. H. Zahiri, "Network: computation in neural systems automatic and heuristic complete design for ANFIS classifier," *Network: Computation in Neural Systems*, vol. 30, no. 1–4, pp. 1–27, 2019.

[23] A. Ansari, I. S. Ahmad, and M. R. Yaakub, "A hybrid metaheuristic method in training artificial neural network for bankruptcy prediction," *IEEE access*, vol. 8, 2020.

[24] B. Xu, X. Wang, J. Zhang, Y. Guo, and A. A. Razzaqi, "A novel adaptive filtering for cooperative localization under compass failure and non-Gaussian noise," *IEEE Transactions on Vehicular Technology*, vol. 71, no. 4, pp. 3737–3749, 2022.

[25] X. Hou, L. Zhang, Y. Su et al., "A space crawling robotic biopaw (SCRBP) enabled by triboelectric sensors for surface identification," *Nano Energy*, vol. 105, Article ID 108013, 2023.

[26] Y. Zheng, X. Lv, L. Qian, and X. Liu, "An optimal BP neural network track prediction method based on a GA–ACO hybrid algorithm," *Journal of Marine Science and Engineering*, vol. 10, pp. 1399–1410, 2022.

[27] Z. Qu, X. Liu, and M. Zheng, "Temporal-spatial quantum graph convolutional neural network based on schrödinger approach for traffic congestion prediction," *IEEE Transactions on Intelligent Transportation Systems*, vol. 24, no. 8, pp. 8677–8686, 2023.

[28] D. A. Abraham and S. Member, "Array modeling of active sonar clutter," *IEEE Journal of Oceanic Engineering*, vol. 33, no. 2, pp. 158–170, 2008.

[29] X. Ma, Z. Dong, W. Quan, Y. Dong, and Y. Tan, "Real-time assessment of asphalt pavement moduli and traffic loads using monitoring data from Built-in Sensors: optimal sensor placement and identification algorithm," *Mechanical Systems and Signal Processing*, vol. 187, Article ID 109930, 2023.

[30] G. Zhou, S. Su, J. Xu, Z. Tian, and Q. Cao, "Bathymetry retrieval from spaceborne multispectral subsurface reflectance," *Ieee Journal of Selected Topics in Applied Earth Observations and Remote Sensing*, vol. 16, pp. 2547–2558, 2023.

[31] C. Wu, M. Khishe, M. Mohammadi, S. H. Taher Karim, and T. A. Rashid, "Retracted article: evolving deep convolutional neutral network by hybrid sine–cosine and extreme learning machine for real-time COVID19 diagnosis from X-ray images," *Soft Computing*, vol. 27, pp. 3307–3326, 2023.

[32] B. Cheng, M. Wang, S. Zhao, Z. Zhai, D. Zhu, and J. Chen, "Situation-aware dynamic service coordination in an IoT environment," *IEEE/ACM Transactions on Networking*, vol. 25, no. 4, pp. 2082–2095, 2017.

[33] H. Xu, J. Zhou, P. G. Asteris, D. J. Armaghani, and M. M. Tahir, "Supervised machine learning techniques to the prediction of tunnel boring machine penetration rate," *Applied Sciences*, vol. 9, no. 18, pp. 1–19, 2019.

[34] J. Chen, Q. Wang, H. H. Cheng, W. Peng, and W. Xu, "A review of vision-based traffic semantic understanding in ITSs," *IEEE Transactions on Intelligent Transportation Systems*, vol. 23, no. 11, pp. 19954–19979, 2022.

[35] A. A. Liu, Y. Zhai, N. Xu, W. Nie, W. Li, and Y. Zhang, "Region-aware image captioning via interaction learning," *IEEE Transactions on Circuits and Systems for Video Technology*, vol. 32, no. 6, pp. 3685–3696, 2022.

[36] G. Zhou, C. Xu, H. Zhang et al., "PMT gain self-adjustment system for high-accuracy echo signal detection," *International Journal of Remote Sensing*, vol. 43, no. 19–24, pp. 7213–7235, 2022.

[37] Y. Deng, W. Zhang, W. Xu, Y. Shen, and W. Lam, "Nonfactoid question answering as query-focused summarization with graph-enhanced multihop inference," *IEEE Transactions on Neural Networks and Learning Systems*, vol. 85, pp. 1–15, 2023.

[38] S. Lu, J. Guo, S. Liu et al., "An improved algorithm of drift compensation for olfactory sensors," *Applied Sciences*, vol. 12, no. 19, p. 9529, 2022.

[39] G. E. Smith, K. Woodbridge, and C. J. Baker, "Multipperspective micro-doppler signature classification," in *Proceedings of the 2007 IET International Conference on Radar Systems*, Edinburgh, UK, October 2007.

[40] S. Yang, Q. Li, W. Li, X. Li, and A. A. Liu, "Dual-level representation enhancement on characteristic and context for image-text retrieval," *IEEE Transactions on Circuits and Systems for Video Technology*, vol. 32, no. 11, pp. 8037–8050, 2022.

[41] S. Lu, Y. Ban, X. Zhang et al., "Adaptive control of time delay teleoperation system with uncertain dynamics," *Frontiers in Neurorobotics*, vol. 16, Article ID 928863, 2022.

[42] R. Mamgain, R. Jain, and D. Deb, "Study and simulation of radar targets' micro-Doppler signature," *2018 International Conference on Radar (RADAR)*, vol. 1, 2018.

[43] C. Clemente, A. Balleri, K. Woodbridge, and J. J. Soraghan, "Developments in target micro-Doppler signatures analysis: radar imaging, ultrasound and through-the-wall radar," *EURASIP Journal on Applied Signal Processing*, vol. 2013, no. 1, 2013.

[44] A. Saffari, S. Zahiri, and M. Khishe, "Automatic recognition of sonar targets using feature selection in micro-Doppler signature," *Defence Technology*, vol. 20, pp. 58–71, 2023.

[45] F. Liu, X. Zhao, Z. Zhu, Z. Zhai, and Y. Liu, "Dual-microphone active noise cancellation paved with Doppler assimilation for TADS," *Mechanical Systems and Signal Processing*, vol. 184, Article ID 109727, 2023.

[46] F. Liu, X. Zhao, Z. Zhu, Z. Zhai, and Y. Liu, "Dual-microphone active noise cancellation paved with Doppler assimilation for TADS," *Mechanical Systems and Signal Processing*, vol. 184, Article ID 109727, 2023.

[47] A. Saffari, S. H. Zahiri, and M. Khishe, "Fuzzy whale optimisation algorithm: a new hybrid approach for automatic sonar target recognition," *Journal of Experimental & Theoretical Artificial Intelligence*, vol. 35, no. 2, pp. 309–325, 2022.

[48] L. Liu, Y. Li, and K. Kuo, "Infant cry signal detection, pattern extraction and recognition," *2018 International Conference on Information and Computer Technologies (ICICT)*, vol. 2018, no. 2, pp. 159–163, 2018.

[49] N. Bao, T. Zhang, R. Huang, S. Biswal, J. Su, and Y. Wang, "A deep transfer learning network for structural condition identification with limited real-world training data," *Structural Control and Health Monitoring*, vol. 2023, Article ID 8899806, 18 pages, 2023.

[50] A. Dogan and D. Birant, "A weighted majority voting ensemble approach for classification," *2019 4th International Conference on Computer Science and Engineering (UBMK)*, vol. 45, pp. 366–371, 2019.

[51] S. A. Manaf, N. Mustapha, N. Sulaiman, N. A. Husin, M. N. Shah Zainuddin, and H. Z. Mohd Shafri, "Majority voting of ensemble classifiers to improve shoreline extraction of medium resolution satellite images," *Journal of Theoretical and Applied Information Technology*, vol. 95, no. 18, pp. 4394–4405, 2017.

[52] S. M. M. R. Ghavidel Aghdam, M. kazemirad hassani Azhdari, and M. Khishe, "Feature extraction from passive sonar data based on the combination of Cepstrum and short-time fourier," *Transformation*, vol. 27, no. 105, pp. 1–10, 2023.

[53] M. Ghavidel, S. M. H. Azhdari, M. Khishe, and M. Kazemirad, "Sonar data classification by using few-shot learning and concept extraction," *Applied Acoustics*, vol. 195, Article ID 108856, 2022.

[54] A. Saffari, S. H. C. A. Zahiri, and M. Khishe, "Fuzzy grasshopper optimization algorithm: a hybrid technique for tuning the control parameters of Goa using fuzzy system for big data sonar classification," vol. 18, no. 1, pp. 1–12, 2022.

[55] A. Saffari, M. Khishe, and S. Zahiri, "Fuzzy-ChOA: an improved chimp optimization algorithm for marine mammal classification using artificial neural network," *Analog Integrated Circuits and Signal Processing*, vol. 111, no. 3, pp. 403–417, 2022.

[56] Y. Wang, L. P. Yuan, M. Khishe, A. Moridi, and F. Mohammadzade, "Training RBF NN using sine-cosine algorithm for sonar target classification," *Archives of Acoustics*, vol. 45, no. 4, pp. 753–764, 2020.

[57] M. R. Mosavi, M. Khishe, M. J. Naseri, G. R. Parvizi, and M. Ayat, "Multi-layer perceptron neural network utilizing adaptive best-mass gravitational search algorithm to classify sonar dataset," *Archives of Acoustics*, vol. 44, no. 1, pp. 137–151, 2019.

[58] M. Khishe and A. Safari, "Classification of sonar targets using an MLP neural network trained by dragonfly algorithm," *Wireless Personal Communications*, vol. 108, no. 4, pp. 2241–2260, 2019.

[59] M. Khishe, M. R. Mosavi, and M. Kaveh, "Improved migration models of biogeography-based optimization for sonar dataset classification by using neural network," *Applied Acoustics*, vol. 118, pp. 15–29, 2017.

[60] M. R. Mosavi, M. Khishe, and A. Ghamgosar, "Classification of sonar data set using neural network trained by gray wolf optimization," *Neural Network World*, vol. 26, no. 4, pp. 393–415, 2016.

[61] R. Ghosh, "Sonar target classification problem," *Machine Learning Models*, vol. 9, no. 1, pp. 247-248, 2020.

[62] E. Cotter and B. Polagye, "Automatic classification of biological targets in a tidal channel using a multibeam sonar," *Journal of Atmospheric and Oceanic Technology*, vol. 37, no. 8, pp. 1437–1455, 2020.

[63] T. J. Sejnowski, "Learned classification of sonar targets using a massively parallel network," *IEEE Transactions on Acoustics, Speech, and Signal Processing*, vol. 36, no. 7, 1988.

[64] D. Tahmoush, "Review of micro-Doppler signatures," *IET Radar, Sonar & Navigation*, vol. 9, no. 9, pp. 1140–1146, 2015.

[65] Y. Yang, J. Lei, W. Zhang, and C. Lu, "Target classification and pattern recognition using micro-Doppler radar signatures," *Proceedings- Seventh ACIS International Conference on Software Engineering, Artificial Intelligence, Network, and Parallel/Distributed Computer, SNPD 2006, including Second ACIS International Worshop on SAWN 2006*, vol. 2006, pp. 213–217, 2006.

[66] V. C. Chen, D. Tahmoush, and W. J. Miceli, *Radar Micro-doppler Signature Processing and Applications Radar Micro-doppler Signatures*, The Institution of Engineering and Technology, London, UK, 2014.

[67] R. P. Gorman and T. J. Sejnowski, "Analysis of hidden units in a layered network trained to classify sonar targets," *Neural Networks*, vol. 1, no. 1, pp. 75–89, 1988.

[68] A. Mir and J. A. Nasiri, "KNN-based least squares twin support vector machine for pattern classification," *Applied Intelligence*, vol. 48, no. 12, pp. 4551–4564, 2018.

[69] R. K. Jade, L. K. Verma, and K. Verma, "Classification using neural network & support vector machine for sonar dataset," *International Journal of Computer Trends and Technology*, vol. 4, pp. 4–2, 2013, http://www.internationaljournalssrg.org.